Few-femtosecond-resolution characterization and suppression of excess timing jitter and drift in indoor atmospheric frequency comb transfer

Jinho Kang, Junho Shin, Chur Kim, Kwangyun Jung, Suhyeon Park, and Jungwon Kim[*]

School of Mechanical, Aerospace and Systems Engineering, Korea Advanced Institute of Science and Technology (KAIST), Daejeon 305-701, South Korea
[*]*jungwon.kim@kaist.ac.kr*

Abstract: We characterize the timing jitter spectral density of the time-of-flight (TOF) in the indoor atmospheric transfer of optical pulse train over 10 decades of Fourier frequency range (10 μHz – 100 kHz) with sub-100-as resolution using a balanced optical cross-correlator (BOC). Based on the well-known theory for atmospheric transfer of a laser beam, we could fit the measured timing jitter power spectral density to the theory and analyze it with a fairly good agreement from 20 mHz to 10 Hz Fourier frequency range. Moreover, we demonstrate that the BOC-based timing stabilization method can suppress the excess fluctuations in timing from >200 fs (rms) to 2.6 fs (rms) maintained over 130 hours when an optical pulse train is transferred over a 76.2-m long free-space beam path in laboratory environment. The demonstrated stabilization result corresponds to 4×10^{-20} overlapping Allan deviation at 117,000s averaging time.

References and links

1. S. M. Foreman, K. W. Holman, D. D. Hudson, D. J. Jones, and J. Ye, "Remote transfer of ultrastable frequency references via fiber networks," Rev. Sci. Instrum. **78**(2), 021101 (2007).
2. O. Lopez, A. Amy-Klein, M. Lours, C. Chardonnet, and G. Santarelli, "High-resolution microwave frequency dissemination on an 86-km urban optical link," Appl. Phys. B **98**(4), 723–727 (2010).
3. K. Predehl, G. Grosche, S. M. F. Raupach, S. Droste, O. Terra, J. Alnis, Th. Legero, T. W. Hänsch, Th. Udem, R. Holzwarth, and H. Schnatz, "A 920-kilometer optical fiber link for frequency metrology at the 19th decimal place," Science **336**(6080), 441–444 (2012).
4. J. Kim, J. A. Cox, J. Chen, and F. X. Kärtner, "Drift-free femtosecond timing synchronization of remote optical and microwave sources," Nat. Photonics **2**(12), 733–736 (2008).
5. K. Jung, J. Shin, J. Kang, S. Hunziker, C. K. Min, and J. Kim, "Frequency comb-based microwave transfer over fiber with 7×10^{-19} instability using fiber-loop optical-microwave phase detectors," Opt. Lett. **39**(6), 1577–1580 (2014).
6. M. Y. Peng, P. T. Callahan, A. H. Nejadmalayeri, S. Valente, M. Xin, L. Grüner-Nielsen, E. M. Monberg, M. Yan, J. M. Fini, and F. X. Kärtner, "Long-term stable, sub-femtosecond timing distribution via a 1.2-km polarization-maintaining fiber link: approaching 10^{-20} link stability," Opt. Express **21**(17), 19982–19989 (2013).
7. B. Sprenger, J. Zhang, Z. H. Lu, and L. J. Wang, "Atmospheric transfer of optical and radio frequency clock signals," Opt. Lett. **34**(7), 965–967 (2009).
8. K. Djerroud, O. Acef, A. Clairon, P. Lemonde, C. N. Man, E. Samain, and P. Wolf, "Coherent optical link through the turbulent atmosphere," Opt. Lett. **35**(9), 1479–1481 (2010).
9. A. Alatawi, R. P. Gollapalli, and L. Duan, "Radio-frequency clock delivery via free-space frequency comb transmission," Opt. Lett. **34**(21), 3346–3348 (2009).
10. R. P. Gollapalli and L. Duan, "Atmospheric timing transfer using a femtosecond frequency comb," IEEE Photon. J. **2**(6), 904–910 (2010).
11. F. R. Giorgetta, W. C. Swann, L. C. Sinclair, E. Baumann, I. Coddington, and N. R. Newbury, "Optical two-way time and frequency transfer over free space," Nat. Photonics **7**(6), 434–438 (2013).
12. L. C. Sinclair, F. R. Giorgetta, W. C. Swann, E. Baumann, I. Coddington, and N. R. Newbury, "Optical phase noise from atmospheric fluctuations and its impact on optical time-frequency transfer," Phys. Rev. A **89**(2), 023805 (2014).

13. V. W. S. Chan, "Free-space optical communications," J. Lightwave Technol. **24**(12), 4750–4762 (2006).
14. J. J. Degnan, "Satellite laser ranging: current status and future prospects," IEEE Trans. Geosci. Rem. Sens. **GE-23**(4), 398–413 (1985).
15. A. Ishimaru, *Wave Propagation and Scattering in Random Media* (Academic Press, New York, NY, 1978).
16. L. C. Andrews and R. L. Phillips, *Laser Beam Propagation through Random Media Second Edition* (SPIE Press, Bellingham, WA, 2005).
17. S. Klingebiel, I. Ahmad, C. Wandt, C. Skrobol, S. A. Trushin, Z. Major, F. Krausz, and S. Karsch, "Experimental and theoretical investigation of timing jitter inside a stretcher-compressor setup," Opt. Express **20**(4), 3443–3455 (2012).
18. P. Cinquegrana, S. Cleva, A. Demidovich, G. Gaio, R. Ivanov, G. Kurdi, I. Nikolov, P. Sigalotti, and M. B. Danailov, "Optical beam transport to a remote location for low jitter pump-probe experiments with a free electron laser," Phys. Rev. Spec. Top-Accel. Beams **17**(4), 040702 (2014).
19. A. M. Kowalevicz, A. Sennaroglu, A. T. Zare, and J. G. Fujimoto, "Design principles of q-preserving multipass-cavity femtosecond lasers," J. Opt. Soc. Am. B **23**(4), 760–770 (2006).
20. V. I. Tatarskii, *The effects of the turbulent atmosphere on wave propagation* (Keter, Jerusalem, 1971).
21. A. N. Kolmogorov, "A refinement of previous hypotheses concerning the local structure of turbulence in a viscous incompressible fluid at high Reynolds number," J. Fluid Mech. **13**(1), 82–85 (1962).

1. Introduction

High-precision time/frequency transfer and remote timing synchronization are indispensable for many important precision scientific and engineering applications such as time and frequency standards, accelerator-based light sources, radio astronomy, optical communication networks, time keeping, navigation, and defense systems. There has been remarkable progress in the remote transfer of time/timing/frequency information, using both continuous-wave (CW) lasers and ultrafast mode-locked lasers, through optical fiber links in the last decade [1–6]. Recently, time/timing/frequency transfer via free-space links has begun to attract more attention as it can provide higher flexibility than fiber links [7–12]: by using free-space transfer, precise time/timing/frequency information can be transferred to remote locations when fiber links cannot be used (e.g., when the used laser wavelength is not suitable for fiber transfer or when a dedicated fiber link cannot be installed between the points of interest). The free-space transfer has high potential for aerospace networks [13] and satellite laser ranging [14] as well.

In the last few years, there have been several important works in free-space transfer of optical and microwave frequency information. Optical and microwave clock signals were transmitted through a 100-m long rooftop atmospheric link using a continuous-wave (CW) diode laser [7] and single-frequency optical carriers were transferred via a 5-km long free-space coherent optical link [8]. These CW laser-based atmospheric transfer methods have a limitation of delivering a single optical or RF frequency. As an alternative, optical pulse trains (frequency combs) from mode-locked lasers can be used for free-space transfer of optical and RF time/timing/frequency information. Microwave clock signals encoded in frequency combs were delivered through 10-m long indoor [9] and 60-m long outdoor atmospheric links [10], where both results demonstrated τ^{-1} dependence of the Allan deviation up to 500 s. More recently, optical two-way time and frequency transfer (TWTFT) with two Er-doped fiber ring lasers, phase-locked by an optical reference cavity, demonstrated reciprocity with 1 fs timing deviation over 2 km free-space link [11]. Further, the excess optical phase noise of a one-way transfer was measured and showed consistence with the atmospheric turbulence theory [12].

In the free-space transfer of optical pulse trains (frequency combs), there are several noise sources that cause excess fluctuations in the time-of-flight (TOF) through the link. Atmospheric turbulence arisen from temporal and spatial random variations in the air refractive index causes beam wander, scintillation, wavefront distortion, and angle-of-arrival jitter for a laser beam propagating through an atmospheric link [15,16]. They will induce intensity and phase/timing fluctuations. Thermal expansion and mechanical vibrations of the free-space optics components will also cause optical path length variations and beam pointing fluctuations. For example, frequency comb transfer through a 60-m outdoor atmospheric link showed excess timing jitter of 600 fs – 2 ps [1 Hz – 100 kHz] depending on weather conditions when the measurement resolution was 93 fs [10]. The pulse train TOF fluctuation is a critical limiting factor not only in free-space time/timing/frequency transfer but also

synchronization between pump and seed pulses in large-scale optical amplifiers or free-electron lasers (FELs), because a long beam path (delay) between pulses can introduce significant amount of jitter and drift compared to the pulsewidth and limit the achievable pump-probe experiment capability [17,18]. Therefore, to improve the performance of free-space optical transfer of optical pulse trains, there is a strong desire for precisely measuring the excess timing jitter and drift in the TOF over a long period of time in a drift-free way, and further actively stabilizing the TOF by a proper feedback control. So far, the resolution and stability have been limited due to the use of direct photodetection for the pulse train TOF measurement.

In this paper, we characterize the timing jitter spectral density of the TOF in indoor free-space transfer of optical pulse train with sub-100-as resolution (in 100-kHz bandwidth) down to 10 µHz Fourier frequency using a balanced optical cross-correlator (BOC) [4]. We could characterize the typical timing jitter and drift characteristics in the ~100-m scale transfer in a laboratory environment over >100 hours. Based on the well-known theory for atmospheric transfer of a laser beam, we could fit the measured timing jitter power spectral density to the theory and analyze it with a fairly good agreement from 20 mHz to 10 Hz Fourier frequency range. Moreover, we demonstrate that timing stabilization method using a BOC can suppress the excess fluctuations in timing from >200 fs (rms) to 2.6 fs (rms), maintained over 130 hours when an optical pulse train is transferred over a 76.2-m free-space beam path. This corresponds to 4×10^{-20} overlapping Allan deviation at 117,000s averaging time.

2. Experimental setup

Figure 1 shows the experimental setup for demonstrating BOC-based TOF characterization and stabilization of an indoor 76.2-m long free-space link. A 78.7-MHz repetition rate, stretched-pulse mode-locked Er-fiber laser with 1565 nm center wavelength and 48 nm bandwidth is used as the optical pulse train source. The output from the oscillator is amplified to 110 mW by an extra-cavity Er-doped fiber amplifier (EDFA), and the resulting pulsewidth is ~570 fs (full-width half-maximum). Part of the input pulse train (~20 mW) is tapped off by a polarization beamsplitter (PBS 1 in Fig. 1) as the reference pulse for the TOF stabilization using the in-loop BOC (BOC 1 in Fig. 1). By tuning the half-wave plate (HWP in Fig. 1), ~10 mW power is tapped off by a second polarization beamsplitter (PBS 2 in Fig. 1) as reference pulse for the out-of-loop timing jitter/drift characterization. After the PBS 2, 80-mW optical pulse train is applied to the free-space link. A bi-convex lens with a 75-cm focal length is used at the beginning of free-space link to optimize beam sizes through the link. In this experiment, to realize a long free-space beam path on a standard optical table, we implemented the free-space link using a multi-pass cavity (MPC) [19] with two 4-m radius-of-curvature (ROC) concave mirrors. 46-time bounces on the MPC mirrors, separated by ~1.53 m, are used to realize a 71.9-m long forward beam path ($1.53 \times (46 + 1) = 71.9$ m). The transverse wind velocity in the MPC is measured to be ~0.02 m/s. The resulting total one-way link length is 76.2 m; the round-trip path is 152.4 m. Due to the limited reflectance (95 to 99%) of the MPC mirrors and the mirrors in the variable optical delay line, one-way link loss is ~75% and the output power from the MPC becomes 20 mW. At the link output, a 50% partial reflector (PR in Fig. 1) is used. Half of the power (10 mW) is transmitted as the link output, and the excess timing jitter and drift of this pulse train is characterized by the out-of-loop BOC (BOC 2 in Fig. 1). The other half (10 mW) is reflected back to the in-loop BOC 1 for link stabilization. Due to the 75% loss, the resulting reflected power to the BOC 1 becomes 2.5 mW. Note that a Faraday rotator (FR in Fig. 1) is placed between PBS 1 and PBS 2 to direct the reflected pulses from the link output toward BOC 1.

When using the optical cross-correlation for TOF characterization and stabilization, it is important to ensure temporal overlap between the reference pulse and the pulse transmitted through/reflected from the end mirror of the link. In this work, we set the one-way link length to the multiple of 20 pulses (3.81 m × 20 = 76.2 m). Further, since the pulse temporal overlap is required for both in-loop and out-of-loop BOCs, there is an additional length requirement: $L_2 = L_1 + L_3$ (in Fig. 1). In order to minimize the uncompensated path length for the out-of-

loop TOF characterization, we minimized L_3 to 1.5 cm. We further set L_1 and L_2 to 13.5 cm and 15 cm, respectively, by making the setup as compact as possible. Note that an Invar board with low temperature coefficient is used for mounting these parts (L_1, L_2, L_3) to minimize the influence of thermal expansions in reference arms for timing comparison. The temporal offset introduced by the Invar board was measured to be 0.75 fs/K in this experiment.
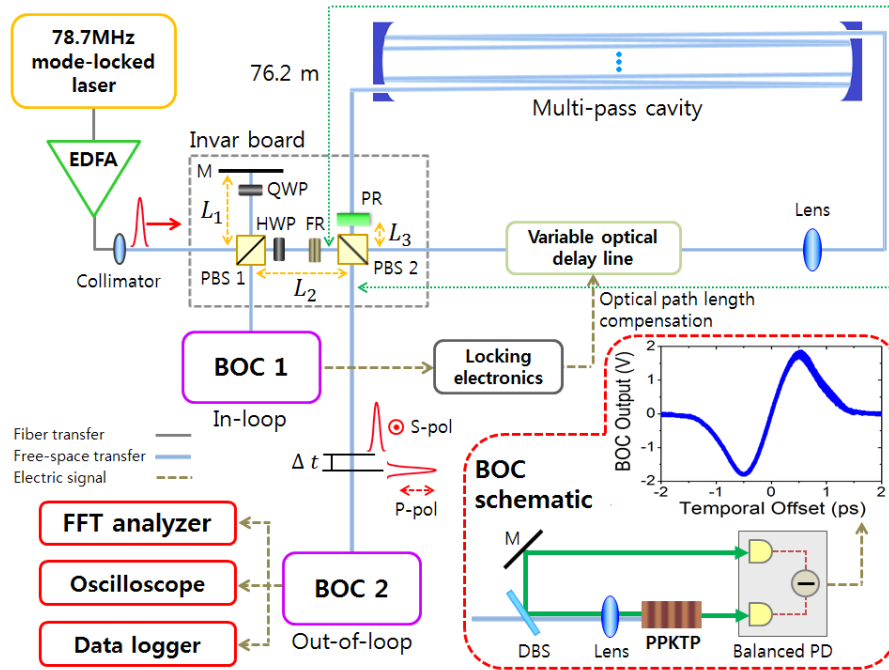

Fig. 1. Experimental setup for the characterization and stabilization of the optical pulse train time-of-flight (TOF) of an indoor 76.2-m long free-space link. BOC, balanced optical cross-correlator. DBS, dichroic beam splitter. EDFA, Er-doped fiber amplifier. FR, Faraday rotator. HWP, half-wave plate. M, mirror. PBS, polarization beamsplitter. PD, photodetector. PPKTP, periodically poled KTP. PR, partial reflector. QWP, quarter-wave plate. Inset shows the measured output from the BOC 2 as a function of temporal offset between pulses before and after the 76.2-m link when changing their relative delay using variable optical delay line.

The excess TOF jitter and drift in the round-trip (152.4 m) and one-way (76.2 m) paths are measured by the in-loop BOC (BOC 1) and out-of-loop BOC (BOC 2), respectively. The BOC detects relative timing between the two orthogonally polarized 1550-nm pulses using a type-II phase-matched PPKTP crystal by generating second-harmonic component depending on the temporal overlap between the two input pulses. More detailed information on the design and construction of PPKTP-based BOC can be found in [4]. Due to the high timing detection sensitivity of nonlinear optic process and low temperature-dependent drift of nonlinear crystals, BOCs can detect the relative timing with both sub-fs resolution and sub-fs long-term stability. The timing error signal generated from BOC 1 is used for TOF stabilization by feeding it back to the variable optical delay line via a locking electronics. The locking electronics in this work consists of a low-pass filter (SRS, SIM965), PI servo (Newfocus, LB1005), and high-voltage amplifier (A. A. Lab Systems Ltd, A-301 HS). The cutoff frequency of the low-pass filter is set to 300 Hz. The variable optical delay line consists of a PZT-stage with 30 μm range (PI, P-840.20) and a motorized stage with 15 mm range (PI, M-111.1DG). One assumption in the TOF stabilization using back-reflected pulses from the link end and bidirectional variable optical delay line is that the fluctuation is slower than the round-trip time, which is easily satisfied for a ~100-m long link as the origins of TOF fluctuations (such as acoustic noise and atmospheric turbulence) are slow processes with <1

kHz bandwidth. The measured timing signal by BOC 2 will evaluate the out-of-loop performance of the link by comparing pulses before and after the 76.2-m free-space link.

3. Measurement results

3.1 Timing drift and Allan deviation

Figure 2 compares the out-of-loop timing drift measurement results in the 76.2-m free-space link using BOC 2 (in Fig. 1), with and without TOF stabilization by BOC 1 (in Fig. 1). Note that, when measuring the timing drift, the BOC 2 output is sampled at 1 sample/s using a data logger (NI, PCI6221) after 1-Hz low-pass filtering. When the TOF is not stabilized [Fig. 2(a)], the long-term fluctuation in timing of free-space link is measured to be ~730 fs (peak-to-peak) in 1 hour, where the drift is mostly induced by thermal expansion as indicated by the measured laboratory temperature change. When the TOF stabilization is turned on [Fig. 2(b)], the resulting timing drift is reduced to 1.6 fs rms (9.8 fs peak-to-peak) over 1 hour even when the temperature change is similar.
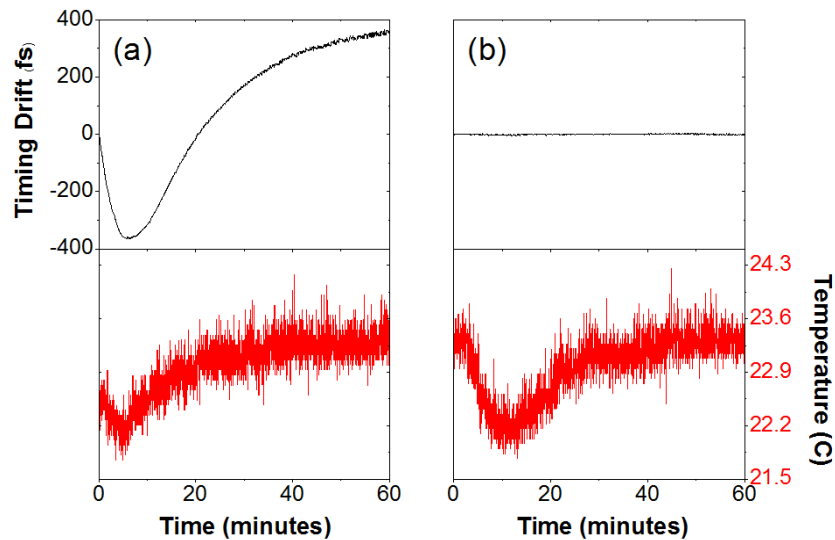

Fig. 2. Out-of-loop timing drift measurement results (a) before and (b) after TOF stabilization.

Figure 3(a) shows a closer look of the out-of-loop timing drift measurement result of the TOF-stabilized link for 130 hours. The resulting rms timing drift is 2.6 fs integrated over 130 hours. The compensated amount of timing fluctuation in the same time span can be obtained from the recorded displacements of PZT and motorized stages in the variable optical delay line: Fig. 3(b) shows that more than 1.3 ps (231 fs) peak-to-peak (rms) drift is compensated by the feedback loop. Note that there are periodic temperature fluctuations with 40 to 90 minutes periods by the air conditioner in the laboratory as shown in Fig. 3(c). The influence of this temperature fluctuation can be found in both the stabilized timing drift result [Fig. 3(a)] and the compensated amount of timing fluctuation result (displacement of PZT and motorized stages, Fig. 3(b)). The BOC-based timing stabilization suppresses the timing drift by a factor of ~100 maintained over >100 hours.
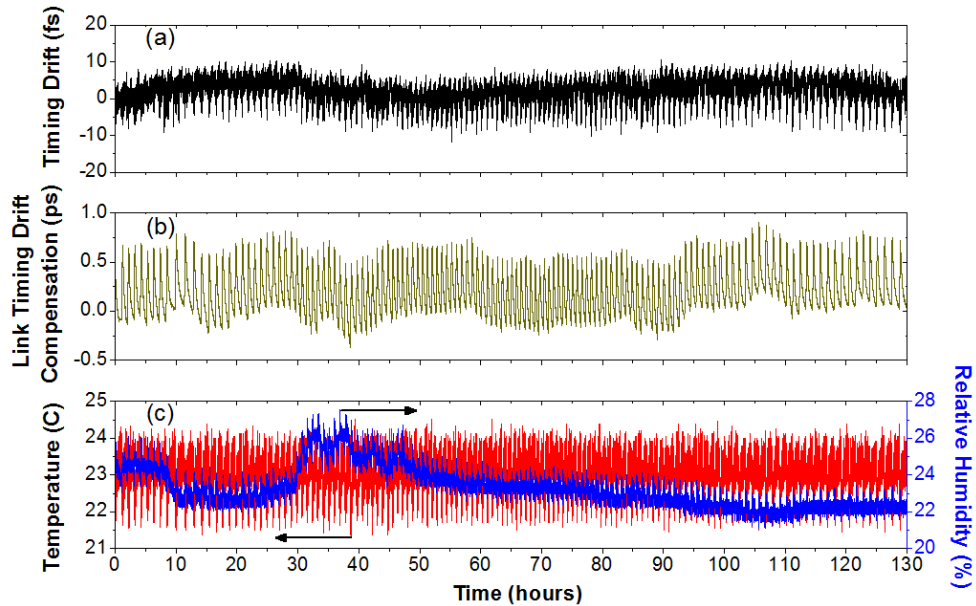
Fig. 3. (a) Out-of-loop timing drift measurement result when BOC-based stabilization is used. (b) The amount of timing drift compensation by PZT and motor stages. (c) Temperature and relative humidity measurement result.
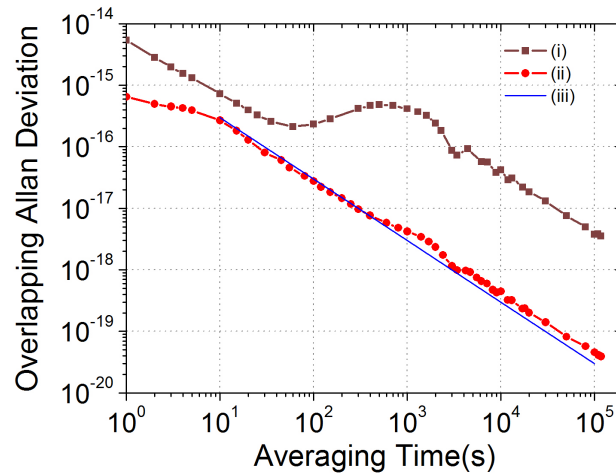

Fig. 4. Fractional frequency uncertainty in terms of overlapping Allan deviation. (i) Without stabilization (calculated from Fig. 3(b) data). (ii) With stabilization (calculated from Fig. 3(a) data). (iii) τ^{-1} slope.

Figure 4 shows the fractional frequency instability in terms of overlapping Allan deviation, calculated from the timing drift measurement results (shown in Figs. 3(a) and 3(b)). Curves (i) and (ii) show the fractional frequency instability before and after TOF stabilization, respectively. When the stabilization is not employed (curve (i)), the Allan deviation shows a broad bump in the range of 100 s to 4000 s averaging time, which reflects the ~800 fs periodic timing fluctuations due to the air conditioner as shown in Fig. 3(b). By using the BOC-based stabilization (curve (ii)), it clearly shows that the fractional frequency instability can be greatly improved by about two orders of magnitude after 1000 s averaging time,

ultimately reaching 4×10^{-20} instability at 117,000 s averaging time. Note that, after 10 s averaging time, the instability nicely scales with the slope of τ^{-1} (curve (iii)), which indicates flicker and white phase noise characteristic. This phase noise characteristic is also confirmed by the computed power spectral density (curve (b) in Fig. 5).

3.2 Power spectral density of timing jitter and drift

Curves (a) and (b) in Fig. 5 show the measured power spectral density (PSD) data of excess timing jitter and drift before and after the TOF stabilization, respectively. From 0.2 Hz to 100 kHz offset frequency, the PSD is measured by the fast Fourier transform (FFT) analyzer; from 10 μHz to 0.2 Hz Fourier frequency (offset frequency), the PSD is obtained by performing the FFT of the 130-hour timing drift measurement results shown in Figs. 3(a) and 3(b). The measured noise floor at ~7×10^{-8} fs^2/Hz above 1 kHz is limited by the background noise in the BOC, mostly originated from the relative intensity noise (RIN) of unwanted type-I-phase-matched second-harmonic component generated from PPKTP. The resulting measurement resolution assuming flat noise floor at ~7×10^{-8} fs^2/Hz is 84 as (rms) over 100-kHz integration bandwidth. If we extend the integration bandwidth up to the Nyquist frequency (39.4 MHz), the projected resolution is 1.7 fs (rms). Curve (c) shows the measurement background noise floor, including the noise equivalent power (NEP) of the used photodetector and the instrument noise floor, when measuring the excess jitter of a short (~65 cm) free-space link. The background noise jitter, integrated from 10 mHz to 100 kHz Fourier frequency, is 100 as (rms). As was also shown in the timing drift measurement results in Fig. 3, the use of BOC-based TOF stabilization greatly suppresses excess timing fluctuation: more than 40 dB is suppressed below 1 mHz Fourier frequency. The resulting rms timing jitter plus drift (integrated from 10 μHz to 100 kHz Fourier frequency) is 1.97 fs and 231 fs with and without TOF stabilization, respectively.
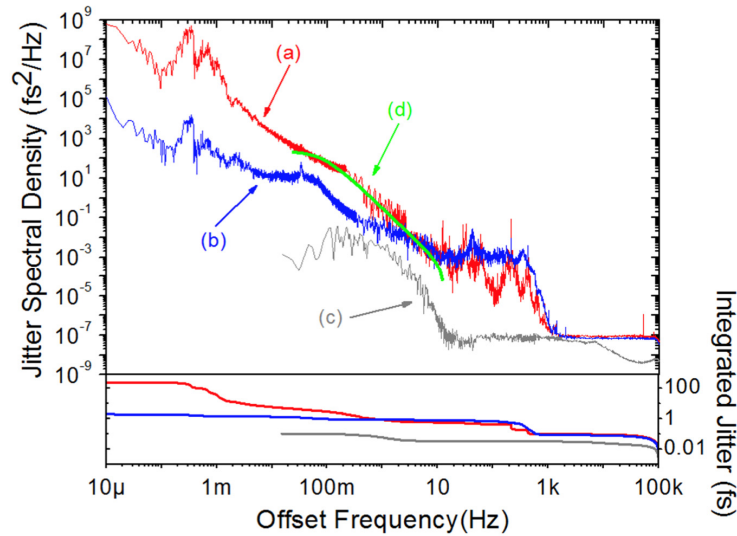

Fig. 5. Power spectral density of the excess timing jitter and drift in the 76.2-m free-space transfer. (a) Without TOF stabilization. (b) With TOF stabilization. (c) Background noise floor of a short link. (d) Fitted curve for atmospheric fluctuations based on the modified Tatarskii spectrum [16].

One interesting finding is that, by plotting the timing noise PSD, we could identify the dominating origins of timing jitter and drift in different time scales. First, in order to evaluate the impact of atmospheric fluctuations in the free-space link, we used a well-established theory of atmospheric turbulence theory [16,20]. Curve (c) shows the theoretical fitting of the atmospheric phase fluctuation contribution for Gaussian beam based on the modified

Tatarskii spectrum shown in [16]. The fitting is based on measured parameters L = 76.2 m (total path length) and v = 0.02 m/s (transverse mean wind velocity). Unlike the straight line-of-sight link, the large-scale size of turbulence eddies, L_0, is assumed to be 1.53 m, which reflects the separation between curved mirrors in the MPC. This short-L_0 assumption (L_0 = 1.53 m) seems reasonable as indicated by the well-fitted roll-off frequency at 82 mHz (= $2\pi v/L_0$) in Fig. 5. The refractive-index structure constant, C_n^2, is estimated to be 4×10^{-14} m$^{-2/3}$ that results in the best fitting in magnitude for 20 mHz – 10 Hz range. The resulting Rytov variance ($\sigma_R^2 = 1.23 C_n^2 k^{7/6} L^{11/6}$, where k is the wavenumber) is 0.007, which is much smaller than 1 and indicates the weak turbulence and weak scintillation regimes. The fitted curve (c) shows a good agreement with the measurement from 20 mHz to 10 Hz range, which indicates that the excess TOF jitter and drift are mainly caused by the atmospheric turbulence effects from ~0.1 s to ~50 s time scale. It further shows the measured timing jitter PSD nicely follows the Kolmogorov's $f^{-8/3}$ power-law from 100 mHz to 10 Hz offset frequency range [12,16,21]. From 10 Hz to 1 kHz offset frequency range, considering the magnitude and shapes of the measured PSD, we believe that mechanical vibrations and acoustic noise coupling to the optomechanics are the dominant TOF fluctuation mechanisms. Note that the experiment is performed on an optical table without any vibration isolation supports. Above 1 kHz, the measurement was limited by the BOC noise floor. Finally, for <20 mHz offset frequency (slower than ~50 s time scale), thermal expansion from temperature fluctuations seems to be dominant for the TOF drift. In particular, the strong peak around 0.3 mHz agrees with the temperature fluctuations with 40-90 minutes periods caused by the air conditioner, as shown in Fig. 3(b). Note that the use of a folded MPC link in this work may have enhanced the susceptibility to vibrations and acoustic noise (in the Fourier frequency above 10 Hz) and thermal expansion (in the Fourier frequency below 20 mHz) compared to a straight-line link.

4. Conclusion and discussion

In summary, based on the BOC method, we characterized the timing jitter and drift PSD down to 10 μHz Fourier frequency with ~100-as resolution (in 100-kHz bandwidth) when transferring optical pulse train through a 76.2-m long atmospheric link in laboratory environment. Based on the PSD measurement, we could identify the dominating origins in the excess timing jitter and drift in different time scales. In this experiment, acoustic noise and vibrations, atmospheric fluctuations, and thermal expansion were dominant factors for TOF fluctuations for <0.1 s, 0.1 s – 50 s, and >50 s time scales, respectively. Our result shows that, thanks to the sub-fs short-term resolution and few-fs long-term stability, the BOC method can be used for precision analysis of the TOF excess jitter and drift in free-space transfer over 10 decades of Fourier frequency range. Further, we could demonstrate that the BOC-based timing stabilization method can suppress the long-term excess timing fluctuation from >200 fs (rms) to 2.6 fs (rms) maintained over 130 hours. The demonstrated stabilization result corresponds to 4×10^{-20} overlapping Allan deviation at 117,000s averaging time. Note that this is the first demonstration of sub-fs-resolution characterization and long-term few-fs-level timing stabilization for free-space transfer. We believe that the current performance can be further improved by the active temperature control of the Invar board and the active beam pointing stabilization.

Our demonstration shows that the BOC method can be readily applicable for the (sub)femtosecond-precision free-space TOF stabilization in laboratory environment. This feature may be useful for large-scale optical amplifiers, ultrafast electron diffraction sources, or FELs with long free-space optical beam paths, where long-term stable (sub)femtosecond-level timing control between optical pulses are required for efficient ultrafast amplification or pump-probe experiments. On the other hand, BOC-based ultrahigh-resolution timing jitter and drift analysis can be performed down to the μHz-level Fourier frequency, which can play an important role in identifying and analyzing the TOF fluctuation mechanisms over atmospheric channels.

In the future we have an interest in applying the demonstrated technique for femtosecond-precision, long-term stable TOF stabilization of outdoor, long-distance atmospheric links.

Due to stronger and more random winds and refractive index changes by temperature fluctuation, outdoor links have much more technical challenges for timing transfer, such as power fluctuations and beam pointing fluctuations. We anticipate that the beam pointing issue can be mitigated by beam pointing control system based on fast steering mirrors (FSMs) [11,12]. Power fluctuation issues may be addressed by monitoring of total reflected power and continuous adjustment of timing detection slope. Our preliminary test shows that there can be ~10% power change when the wind velocity is changed inside the MPC. In this condition, the measured BOC timing detection sensitivity varies ~10% as well, essentially following the total reflected power level. Thus, we may be able to calibrate the BOC sensitivity as a function of total output optical power in a continuous way using a predetermined BOC sensitivity look-up table. Finally, to overcome the limited timing detection range of BOC (up to ~1-2 ps), our recently demonstrated fiber-loop optical-microwave phase detector (FLOM-PD) [5] may be applicable with larger timing detection range (>tens ps) and sub-fs resolution/stability.

Acknowledgment